

**Fundamentals of High Temperature Processes**

**Potentialities of simultaneous removal of tin and copper from molten iron through evaporation**  
A.I.ZAITSEV *et al.*

The Knudsen-cell mass spectrometry was used to study evaporation and thermodynamics of pure liquid Sn, Fe-Sn and Fe-Cu-Sn molten alloys containing up to 20.3 mol% Sn or up to 5 mol% Cu and Sn in a wide temperature range. The thermodynamic properties of the binary melt were approximated by means of the subregular solution model with temperature dependent parameters. The properties of the ternary melt were represented with accuracy not worse than the experimental one by combination of the characteristics of the binary constituents. The obtained results were applied to assessment of the potentialities of simultaneous copper and tin removal from molten steel by means of evaporation. Combination of vacuum treatment of a 160-tons ladle with blowing through the molten metal neutral gases was considered as an example. Two processes are responsible for removal of copper and tin: transfer into gas bubbles, free-rising from the ladle bottom to its surface, and evaporation from molten metal surface, turbulized by blowing-through gas. It was shown that duration of the treatment necessary for a decrease in Cu concentration from 0.6 to 0.3 wt% amounts to ~1.5 h and is not practically affected by variations in tin content in the range of 0.01 to 0.6 wt%. During this time concentration of tin changes insignificantly at any initial content: from 0.6 to ~0.51, from 0.1 to ~0.086 or from 0.01 to ~0.0086 wt%.

(cf. *ISIJ Int.*, **44** (2004), 957)

**Critical thermodynamic evaluation and optimization of the CaO-MnO-SiO<sub>2</sub> and CaO-MnO-Al<sub>2</sub>O<sub>3</sub> systems**

Y.-B.KANG *et al.*

A complete review, critical evaluation, and thermodynamic optimization of phase equilibrium and thermodynamic properties of the CaO-MnO-SiO<sub>2</sub> and CaO-MnO-Al<sub>2</sub>O<sub>3</sub> systems at 1 bar pressure are presented. The molten oxide phase was described by the Modified Quasichemical Model, the Gibbs energy of the olivine solid solution was modeled with the Compound Energy Formalism, and the wollastonite s.s., rhodonite s.s., and  $\alpha$ - and  $\alpha'$ -Ca<sub>2</sub>SiO<sub>4</sub> solutions were modeled by polynomial expansions of the excess Gibbs energy. Sets of optimized model parameters for all phases were obtained which reproduce all available reliable thermodynamic and phase equilibrium data within experimental error limits from 25°C to above the liquidus temperatures over the entire ranges of composition. The liquidus surface of the CaO-MnO-Al<sub>2</sub>O<sub>3</sub> system, which has not been measured, has been predicted. Complex phase relationships in these systems have been elucidated, and discrepancies among the data have been resolved. Phase equilibria between liquid slag and manganese alloys have been calculated. The database of model parameters can be used along with software for Gibbs energy minimization in order to calculate any phase diagram section or thermodynamic property.

dynamic property.

(cf. *ISIJ Int.*, **44** (2004), 965)

**Phase equilibria and thermodynamic properties of the CaO-MnO-Al<sub>2</sub>O<sub>3</sub>-SiO<sub>2</sub> system by critical evaluation, modeling and experiment**

Y.-B.KANG *et al.*

A complete literature review, critical evaluation and thermodynamic modeling of phase diagrams and thermodynamic properties of the CaO-MnO-Al<sub>2</sub>O<sub>3</sub>-SiO<sub>2</sub> system at 1 bar pressure are presented. A few new quaternary liquidus measurements are also reported. The modeling is based solely upon model parameters obtained by critical evaluation and optimization of the four ternary subsystems. The predicted quaternary properties and phase diagrams are in very good agreement with measurements. Complex phase relationships are elucidated and discrepancies among the data are resolved. The database of model parameters can be used along with software for Gibbs energy minimization in order to calculate any phase diagram section or thermodynamic property from 25°C to above the liquidus at all compositions.

(cf. *ISIJ Int.*, **44** (2004), 975)

**Rate of iron carbide formation from reduced iron in CO-H<sub>2</sub>-H<sub>2</sub>S mixtures under pressurized conditions**

Y.IGUCHI *et al.*

Under pressurized conditions up to 0.6 MPa, the rate of the iron carbide formation from completely reduced iron in CO-H<sub>2</sub>-H<sub>2</sub>S mixtures was measured by gravimetric technique. The fractional conversion for carbide formation,  $f_{\theta}$ , was defined as the weight gain divided by the weight of carbon for the complete conversion to cementite. First, the compositions of the partially reacted samples were analyzed by Mössbauer absorption spectroscopy. Then, the fractional conversion calculated from the composition,  $f_{\theta}^M$ , was compared with  $f_{\theta}$ . The value of  $f_{\theta}$  agreed reasonably with that of  $f_{\theta}^M$  in the range  $f_{\theta} < 0.8$ , from which the gravimetric method is proved to be valid to the measurements for the rate of iron carbide formation. The carbide formation curves,  $f_{\theta}$  versus  $t$  relation, were not influenced by the weight of the sample and the flow rate of the reaction gas in the conditions; 50 mg, more than  $3.33 \times 10^{-6}$  m<sup>3</sup>/s. Cross sectional view indicated the homogeneous distribution of cementite regions in the reduced iron particles partially converted to cementite. On the other hand, the rate was very sensitive to the conditions of the carburization reaction on the pore surface. The rate increased with increasing the content of carbon monoxide up to 80 to 90%, where the rate was the maximum, and then gradually decreased with further increasing the content. The rate increased with the total pressure, but decreased with the activity of sulfur. The rate controlling step of the iron carbide formation was discussed on the basis of the experimental results. The rate controlling step was assumed to be the carburization reactions on the pore surface of reduced iron particles.

(cf. *ISIJ Int.*, **44** (2004), 984)

**Kinetics of cementite formation from reduced iron in CO-H<sub>2</sub>-H<sub>2</sub>S mixtures under pressurized conditions**  
Y.IGUCHI *et al.*

In the present authors' previous study, the rate of iron carbide formation from completely reduced iron ore was gravimetrically measured in CO-H<sub>2</sub>-H<sub>2</sub>S mixtures of sulfur activity 0.035 to 0.6 at the total pressure of 0.1 to 0.6 MPa and at the temperature of 773 to 1023 K. From the experimental results under the wide conditions, it was derived that the rate of iron carbide formation was controlled by the carburization reaction on the pore surface of reduced iron. In this study, the integrated rate equation for the first order reaction,  $-\ln(1-f_{\theta}) = g(p, T)t$ , was applicable to cementite formation curves,  $f_{\theta}$  versus  $t$  relation, in the range of iron carbide formation, i.e.  $f_{\theta} < 0.6$ . The value of  $g(p, T)$  is proportional to the partial pressure of carbon monoxide,  $p_{CO}$ , in the reaction gas containing hydrogen more than 20%. From the dependency of  $g(p, T)$  on  $p_{CO}$ , it was assumed that the rate controlling elementary reaction for the carburization of reduced iron is the dissociative adsorption of carbon monoxide on the pore surface. Following the elementary reaction, the rate equation for the carburization was derived substituting the adsorption isotherm for sulfur;  $g(p, T) = k_{CO}(p_{CO} - a_C p_{H_2O}/K_S p_{H_2}) / (1 + K_S a_S)$ . The relation between  $p_{CO}/g(p, T)$  and  $a_S$  derived by rearranging the rate equation was applied to the data for  $g(p, T)$  to obtain  $k_{CO}$  and  $K_S$ . At the individual temperatures, the good linear relation was observed. The temperature functions for  $k_{CO}$  and  $K_S$  were obtained. The rate equation substituted with the values of  $k_{CO}$  and  $K_S$  for the carburization simulated reasonably well the carbide formation curves in the range  $f_{\theta} < 0.6$ .

(cf. *ISIJ Int.*, **44** (2004), 992)

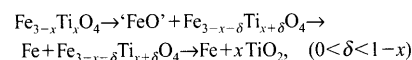
**Ironmaking**

**Reduction of titania-ferrous ore by hydrogen**

E.PARK *et al.*

The reduction of titania-ferrous ore (ironsand) containing 57.2 mass% of iron and 7-8 mass% of TiO<sub>2</sub> was investigated in isothermal experiments using H<sub>2</sub>-Ar gas mixtures in a laboratory fixed bed reactor in the temperature range from 973 to 1373 K. The degree of reduction was measured using an on-line Dew Point sensor and the samples in the course of reduction were characterized using SEM and XRD analyses.

The complete reduction of iron oxide in the ore by 25vol% H<sub>2</sub>-Ar was achieved within 60 min at temperature higher than 1123 K. At 1173 K, the reduction rate increased with hydrogen content in the reducing gas up to 25 vol% H<sub>2</sub>. The composition of samples after 2-h reduction by 25vol% H<sub>2</sub>-Ar depended on the reduction temperature. Below 1073 K, the final sample contained iron and iron-titanium oxides. At temperatures above 1173 K, the final sample was composed of iron and titanium oxide. The reduction path at temperatures above 1173 K is suggested as follows:



(cf. *ISIJ Int.*, **44** (2004), 999)

## Steelmaking

### Inclusions chemistry for Mn/Si deoxidized steels: thermodynamic predictions and experimental confirmations

Y.-B.KANG *et al.*

Inclusions chemistry of Mn/Si deoxidized steel was studied through both thermodynamic computation and experimental method. The computational thermodynamics has proved to provide a powerful tool for controlling inclusions and precipitates in steel. For Mn/Si deoxidized steels, important factors in determining the liquidus temperature and primary phase of the inclusions are MnO/SiO<sub>2</sub> ratio and Al<sub>2</sub>O<sub>3</sub> content in inclusions. Provided that no further interaction with steel matrix during cooling, inclusions having MnO/SiO<sub>2</sub> mass% ratio near unity and Al<sub>2</sub>O<sub>3</sub> content in the range of 10–20 mass% give low liquidus temperatures (1150–1200°C) and primary phases of MnSiO<sub>3</sub> and Mn<sub>3</sub>Al<sub>2</sub>Si<sub>3</sub>O<sub>12</sub> both which are soft. For the case of Mn+Si=1.0 in mass%, the Mn/Si ratio of 2–5 meets the above conditions. Effect of the top slag on the inclusions chemistry can be predicted with accuracy, and hence it is possible to control the inclusions chemistry through proper design of the top slag composition so that the inclusions show a low liquidus temperature and soft primary phase. As the inclusions composition gradually changes with time toward the top slag composition, the length of refining time which determines the extent of reaction with the top slag is an important factor in determining the inclusions chemistry.

(*cf. ISIJ Int.*, **44** (2004), 1006)

### Effect of Al on the evolution of non-metallic inclusions in the Mn–Si–Ti–Mg deoxidized steel during solidification: Experiments and thermodynamic calculations

S.-C.PARK *et al.*

The effect of Al on the evolution of non-metallic inclusions in the Mn–Si–Ti–Mg deoxidized steels during solidification were investigated based on the experiments and thermodynamic calculations. The inclusions belonged to the MgO–TiO<sub>2</sub>–Ti<sub>2</sub>O<sub>3</sub>–Al<sub>2</sub>O<sub>3</sub>+MnS+TiN system. In particular, the major oxide inclusion was the Mg–Ti–Al–O spinel phase of which composition was continuously changed from the Mg–Ti–O to MgAl<sub>2</sub>O<sub>4</sub> with the concentration Al in steels. The spinel compositions calculated from thermodynamic databases are in good agreement with experimental results. TiN was only observed on the surface of MnS. MgAl<sub>2</sub>O<sub>4</sub> aggregates were also observed at high Al concentration. In general, the evolution of inclusions is well explained by thermodynamic calculations.

(*cf. ISIJ Int.*, **44** (2004), 1016)

## Casting and Solidification

### Analysis of fluid flow turbulence in tundishes fed by a swirling ladle shroud

G.SOLORIO-DIAZ *et al.*

A new design of a ladle shroud, obtained through water modeling, that controls turbulence of the entry

jet in continuous casting tundishes is proposed. Particle Image Velocimetry (PIV) measurements indicate that this design decreases the impact velocity on the tundish bottom to close to 1/3 of that provided by a conventional ladle shroud. This achievement is due to a swirling jet that promotes a recirculatory flow in the horizontal planes of the tundish. The swirling effects help to dissipate the turbulence energy of the jet before it impacts the tundish bottom making possible decreases of fluid velocities that impact the back and front walls of the tundish. Turbulence models like *k*–*ε*, *k*–*ω* and RSM were applied to simulate the experimental PIV measurements of velocities in the fluid flow. Only the RSM model yielded results that agree remarkably well with the experimental determinations. These results make possible to avoid the employment of flow control devices such as dams, weirs, turbulence inhibitors and the like in tundishes.

(*cf. ISIJ Int.*, **44** (2004), 1024)

## Chemical and Physical Analysis

### Ferrite–martensite steels characterization using magnetic Barkhausen noise measurements

X.KLEBER *et al.*

Magnetic Barkhausen noise measurements have been carried out to characterize Ferrite-Martensite steels. Using thermal treatments, the volume fraction and the carbon content of martensite were varied in reasonable proportions. The results indicate that the Barkhausen noise measurements can easily allow us to distinguish the two phases, ferrite and martensite. Using a simple mixture rule, we found a good correlation between the martensite volume fraction and the Barkhausen noise amplitude. We observed that the value of the magnetic field for which the Barkhausen noise peak is obtained, correlates with the carbon content of martensite.

We demonstrated that it was possible to use Barkhausen noise measurement to determine both the relative proportion of the two phases (ferrite and martensite) and the carbon content of martensite. The use of this technique could be extended to characterize industrial Dual-Phase steels.

(*cf. ISIJ Int.*, **44** (2004), 1033)

## Forming Processing and Thermomechanical Treatment

### Traditional Japanese sword making from a tataru ingot as estimated from microstructural examination

J.-S.PARK

This paper has examined the progressive development of microstructures in the iron and steel samples taken at several different stages in the traditional Japanese sword making from a Tataru ingot. The results show that the use of a particular input material, Tataru steel, and the adoption of the manufacturing technique, repeated cycles of forging and folding, may be the major factors characterizing the sword making. The undesirable aspects of both the heterogeneous Tataru ingot and the labor-intensive forge/fold operation are found complemented in

their combination. It is shown that this combination provides an effective control over the compositional and microstructural variations inherent in the Tataru steel while it is shaped into a sword. The finished sword comes thereby to achieve fairly uniform structures, at least, macroscopically with the earlier variation still retained in the form of fine layered microstructures. The present study shows that the key role of forging in achieving the desired effects can be understood only if the dynamic evolution of microstructure from one stage to another is carefully examined because majority of the structural developments in the forging process have only a transient existence. Besides, they often hold crucial information relating the Japanese sword making to the general technical traditions of East Asia where cast iron has been playing an important role since the inception of iron-working. This article will detail the continuous microstructural development in the entire process of the traditional Japanese sword making, without which its technical and historical facets cannot be properly recognized.

(*cf. ISIJ Int.*, **44** (2004), 1040)

### Collision dynamics of two droplets impinging successively onto a hot solid

H.FUJIMOTO *et al.*

The collision of two successive water droplets with a hot solid was investigated. Experiments were carried out on water droplets with a diameter of approximately 0.6 mm and an impact velocity of 3.5 m/s at various droplet spacing and time intervals. The temperature of the solid surface was set at 120, 300, and 500°C. The Weber number, based on the pre-impact diameter of droplet and the impact velocity, is approximately 100. At low surface temperature (120°C), the coalesced liquid is deformed into the shape of a crown with its height increasing with droplet spacing. The hydrodynamics of the formation process of the crown is also studied in detail by numerical simulations under isothermal conditions. For the cases of 300 and 500°C, the coalesced liquid breaks up into small droplets as boiling occurs at the liquid–solid interface. The time evolution of droplet shape is dependent on the surface temperature as well as the spacing between two droplets.

(*cf. ISIJ Int.*, **44** (2004), 1049)

## Transformations and Microstructures

### Effect of heat treatment on microstructures and tensile properties of ultrafine grained C–Mn steel containing 0.34 mass% V

K.-T.PARK *et al.*

An ultrafine grained (UFG) C–Mn steel containing a relatively large amount of vanadium was fabricated by equal channel angular pressing (ECAP) and its microstructures and tensile properties were examined. This investigation was aimed at demonstrating the effect of precipitation stage of vanadium precipitates in the course of the material processing on the tensile properties of the ultrafine grained C–Mn steel, especially strength and strain hardening capability. For this purpose, the two different heat treatments were carried out on the present steel: (a)

conventional normalization for vanadium precipitation before ECAP, and (b) isothermal transformation for vanadium precipitation during ECAP and subsequent annealing. The results showed that the second heat treatment was more effective on improving the thermal stability and the overall tensile properties of the steel by better uniform distribution of nano-sized vanadium precipitates which yielded an extensive interaction with lattice dislocations inside ultrafine ferrite grains. In addition, in this report, the feasibility enhancing the strain hardening capability of the UFG C–Mn steel was explored by comparing the microstructure and stress–strain curve of the steel prepared by the second heat treatment with those of the UFG C–Mn steel without vanadium.

(cf. *ISIJ Int.*, **44** (2004), 1057)

### Strain-hardening due to dispersed cementite for low carbon ultrafine-grained steels

*A. OHMORI et al.*

Strain(work)-hardening in tensile tests was examined for low carbon steels with various ferrite grain sizes ranged from 0.4 to 16  $\mu\text{m}$ . The steels had microstructures composed of ferrite grains and dispersed cementite particles. They were fabricated through warm caliber bar-rollings with an accumulative area reduction of 93%.

Strain-hardening rate at a given strain increased with an increase in volume fraction of cementite particles. The balance of yield strength and uniform elongation for ultrafine-grained structures could be improved by the dispersion of cementite particles. Effects of the cementite dispersion and the ferrite grain size on the strain-hardening rate can be roughly explained by the work-hardening model with GN-dislocation density. Strain-hardening design using dispersed cementites was proved to be effective in controlling ductility of the ultrafine-grained steels.

(cf. *ISIJ Int.*, **44** (2004), 1063)

### The influence of solute carbon in cold-rolled steels on shear band formation and recrystallization texture

*M.D. NAVE et al.*

Two experiments were conducted to clarify the roles of grain size, solute carbon and strain in determining the recrystallization textures of cold-rolled and annealed steels. In the first experiment, samples of coarse-grained low-carbon (LC) and interstitial-free (IF) steels were cold-rolled to a 75% reduction in thickness. One sample from each steel was polished and cold-rolled an additional 5%, while the remaining samples were annealed for various times at 650°C. In the second experiment, three samples from a commercial LC steel sheet were rolled 70% at 300°C. Two of the samples were given a further rolling reduction of 5% of the original thickness, with one of the samples being given this additional reduction at 300°C and the other at room temperature. Goss recrystallization textures are strengthened by coarse initial grain sizes, the presence of solute carbon and rolling at a temperature where dynamic strain ageing occurs, but are weakened by additional rolling beyond a reduction of 70%, especially when this extra rolling is conducted at a temperature

where dynamic strain ageing does not occur. Characterization of key features of the deformed and recrystallized steels using optical microscopy, scanning electron microscopy (SEM) and electron backscatter diffraction (EBSD) supports a rationale for these effects based on the repeated activation and deactivation of shear bands and the influence of solute carbon and dynamic strain ageing on the operating life of the bands and the accumulation of strain within them.

(cf. *ISIJ Int.*, **44** (2004), 1072)

### A kinetics model of isothermal ferrite and pearlite transformations under applied stress

*J.S. YE et al.*

A modified kinetics model of ferrite and pearlite transformations under applied stress is proposed based on the Johnson–Mehl–Avrami (J–M–A) equation and is shown as  $f=1-\exp[-b(\bar{\sigma})^m t^n]$ , in which  $b(\bar{\sigma})=b(0)(1+A\bar{\sigma}^B)$  and  $n(\bar{\sigma})=n(0)$ . The parameters  $A$  and  $B$  in the suggested model were determined by regression of the data from experiments in a 0.38C–Cr–Mo steel and a eutectoid carbon steel. The calculation results of the two steels show that the suggested model can precisely predict the onset and the end of ferrite and pearlite transformations under applied stress. The effect of applied stress on ferrite or pearlite transformation is remarkable and the constants  $A$  and  $B$  in the suggested model vary with the different steels and different transformations.

(cf. *ISIJ Int.*, **44** (2004), 1079)

### Secondary recrystallization behavior in 3% Si grain oriented steels

*S.K. CHANG et al.*

The effects of primary recrystallization on secondary recrystallization in grain oriented 3% Si steels were experimentally clarified and unidentified microstructural behavior in the incubation stage of secondary recrystallization was verified. A secondary recrystallization mechanism from the incubation period to the growth stage is suggested by identifying microstructural changes based on grain orientation, texture, and misorientation.

(cf. *ISIJ Int.*, **44** (2004), 1086)

### The effects of vanadium, niobium, titanium and zirconium on the microstructure and mechanical properties of thin slab cast steels

*Y. LI et al.*

The evolution of precipitation and microstructure during a simulation of the thin slab direct rolling process, in six vanadium based, low carbon, steels with V, V–N, V–Ti–N, V–Nb, V–Nb–Ti and V–Zr additions was studied by optical microscopy, analytical transmission electron microscopy (TEM), energy dispersive X-ray analysis (EDAX) and parallel electron energy loss spectroscopy (PEELS). Tensile properties and Charpy vee-notch toughness of the final strip were also determined. The effects of microalloying additions and processing conditions, including equalisation temperature (1200°C, 1100°C and 1050°C) and end water cool temperature, on the

austenite and ferrite grain sizes, as well as the type and composition of the precipitates, were determined. The relationship between the microstructure and the properties in the steels was also ascertained.

(cf. *ISIJ Int.*, **44** (2004), 1093)

## Mechanical Properties

### Thermal fatigue behavior of new type High-Cr Cast Hot Work Die Steel

*Q.C. JIANG et al.*

The thermal fatigue (TF) behavior of a new type high-Cr cast hot work die steel was investigated. The results indicate that TF cracks initiate at the grain boundaries or at the interface between inclusion and matrix, which had been oxidized, and then propagated along the grain boundaries. The thermal fatigue crack initiation and propagation have been accelerated greatly by oxidation. The new type cast high Cr hot work die steel has a better thermal fatigue resistance compared to 4Cr5MoSiV1(8407) steel under thermal cycling temperatures of 650–25°C. Good oxidation and temper resistances are the main causes for the better TF resistance of the new type high-Cr cast hot work die steel.

(cf. *ISIJ Int.*, **44** (2004), 1103)

### Fuzzy model-based Charpy impact toughness assessment for ship steels

*M.-Y. CHEN et al.*

The present research aims at linking steel composition and microstructure to a prediction of Charpy impact properties of ship structural steel, including Charpy impact energy, transition temperature (ITT) and fracture appearance (brittleness). In this paper, adaptive fuzzy modelling techniques were applied to develop generic models for the prediction of Charpy impact properties of Grade A and AH36 ship steels. Using the proposed fuzzy modelling approach, the rule-based fuzzy prediction models, which involved chemical composition, grain size, tensile strength and Charpy impact energy, were generated and optimised automatically from numerical data. The investigation of the relationship between Charpy impact energy and fracture surface characteristics is also presented in the paper. Numerical analysis shows that using the obtained fuzzy models we are able to predict Charpy toughness for given steel compositions and microstructures, and also reveal useful qualitative information linking composition–microstructure to Charpy impact properties.

(cf. *ISIJ Int.*, **44** (2004), 1108)

### The effect of cold work and fracture surface splitting on the charpy impact toughness of quenched and tempered steels

*Z. STERJOVSKI et al.*

Quenched and tempered (QT) steels are commonly used in the manufacture of transportable pressure vessels in Australia. During the weld fabrication process sections of the head and shell are cold formed (2–5% strain) prior to welding. The effect of this plastic strain on the impact toughness of the base (parent) plate is commonly overlooked because

mandatory postweld heat treatment (PWHT) is likely to counteract any effects of cold work. However, since the PWHT of QT steels for transportable pressure vessels is currently under review in Australia, it is pertinent to consider the effect of cold work on impact toughness.

This paper specifically reports on the effect of 3.5% total strain (~3.2% plastic strain) on the impact energy values of 12 mm 700 grade QT steel. This steel, although not currently classified as a pressure vessel steel, is being considered as a poten-

tial steel for transportable pressure vessels based on its superior impact and fracture toughness to 700PV grade (currently used for transportable pressure vessels). It was found that a permanent strain of 3.2% significantly reduced the impact toughness of the 12 mm 700 grade steel, and that PWHT (545°C) resulted in recovery of the impact energy to a level similar to that for PWHT of non-cold worked steel.

This paper also reports on the role of splitting on the impact energy values of 700PV grade (11 and 20 mm) and 700 grade (12 mm) steels. Reports in

the literature and the current work suggest that steels with a tendency to split record impact energy values significantly lower than similar steels that do not exhibit splitting. However, when other variables are kept constant, an increased incidence of splitting of the Charpy fracture surface was found to be associated with higher impact energy values. It is concluded that variable degrees of splitting is a major contributor to the well-known scatter in impact test results.

(cf. *ISIJ Int.*, **44** (2004), 1114)